ACS OMEGA

Article

Cite This: ACS Omega 2019, 4, 606−619

http://pubs.acs.org/journal/acsodf

Phe−Phe Di-Peptide Nanostructure Self-Assembling Modulated by Luminescent Additives

Antonio C. C. Ribeiro,[†] Geovany A. Souza,[†] Douglas Henrique Pereira,[‡] Diericon S. Cordeiro,[†] Ramon S. Miranda,[†] Rogério Custódio,[§] and Tatiana D. Martins*[,†]

[†]Chemistry Institute, Federal University of Goias, Campus II—Samambaia, P.O. Box 24242, Goiania 74690-970, Brazil

[‡]Chemistry Collegiate, Federal University of Tocantins, Campus Gurupi-Badejós, P.O. Box 66, Gurupi 77 402-970, Brazil

[§]Institute of Chemistry, University of Campinas, Barão Geraldo, P.O. Box 6154, Campinas 13083-970, São Paulo, Brazil

Supporting Information

ABSTRACT: In this work, supramolecular L-L-diphenylalanine (Phe−Phe) nanostructures were self-assembled in solvents of distinct polarity and in the presence of luminescent additives of distinct conjugation length that physically adhere to the nanostructures to provide growth environments of distinct properties. When the additive is poly[2-methoxy-5-(2-ethylhexyloxy)-1,4-phenylenevinylene], an electron donor polymer, and solvent is tetrahydrofuran (THF), Phe−Phe vesicle-like structures are obtained, whereas in water and in the presence of a similar additive in structure, poly[5-methoxy-2-(3-sulfopropoxy)-1,4-phenylenevinylene], nanotubes are formed. In contrast, when 9-vinyl-carbazole, an electron acceptor additive is used, nanotubes are formed even when THF is the solvent. The same structures are obtained when the additive is the macromolecule poly(vinyl carbazole). The morphologies of these self-assembled structures were observed by scanning electron microscopy, and their photophysical behavior was determined by steady-state fluorescence spectroscopy and time-resolved fluorescence spectroscopy. These data analyzed altogether inform about the formation mechanisms of such structures and about the influence that distinct interactions exert on self-assembling and charge-transfer processes through formation of complexes between the luminescent additives and the Phe−Phe nano- and microstructures.

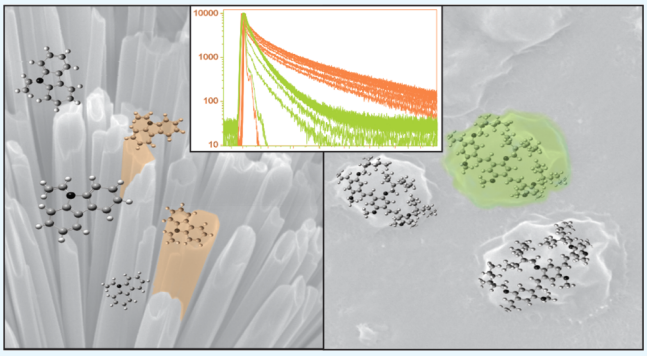

INTRODUCTION

Supramolecular bottom-up strategies are based on direct synthesis of nanoparticles and enable particle size and shape control by the modulation of preparation conditions.[1−5] By these approaches, a wide range of nanostructures can be produced using any type of material, from simple inorganic compounds to complex organic systems.[6−13] Supramolecular approaches also enable the understanding of the formation processes of such structures and the identification of the associated inter- and intramolecular driving forces that result in new structures. Therefore, experimental conditions and procedures can be designed in order to achieve the desired structures.[14]

Among the most prominent nanomaterials that find applications in science and technology are the sp^2 carbon-based structures, which can present distinct morphologies upon preparation methods, such as single- or multiwalled nanotubes (carbon nanotube, CNT),[15−18] fullerenes,[19] or graphenes.[20] Each of these structures presents peculiar properties that find several technological applications, such as thermal and chemical resistance, flexibility, and electric charge transport, the last enabling them to act in charge-transfer processes. Specially, CNTs present optical, magnetic, and optoelectronic properties beyond the expected for such simple carbon aggregation, raising the question on whether other organic compounds could present interesting properties when self-assembled into similar structures. In this context, peptide nanotubes are thought to be alternatives for the use of carbon structures, such as those reported by Ghadiri et al.,[21,22] in which L-L-diphenylalanine (Phe−Phe) assumes a bidimensional ring configuration. In such array, Phe−Phe rings pack in an antiparallel way, interacting with each other to give a β-sheet structure.

Although several peptides have been employed to describe the forces involved in self-assembling,[12,23−27] the interest devoted to Phe−Phe is due to its ability to self-assemble into distinct structures, depending on the experimental procedures adopted and the unique properties presented by each structure.[28−30] With regard to it, Reches[31] and Gazit[32] showed that Phe−Phe derivatives self-assemble into nanotubes when

Received: October 9, 2018
Accepted: December 26, 2018
Published: January 9, 2019

DOI: 10.1021/acsomega.8b02732
ACS Omega 2019, 4, 606−619

water is the solvent. Also, Gorbitz[33] showed that Phe−Phe nanotubes present a hexagonal organization in which the inner channels are hydrophilic, whereas the external walls are hydrophobic.

By doping these structures with a variety of additives, their already surprising properties can be greatly improved to supply the needs for new and extraordinary materials for scientific and technological applications.[34−40]

Poly[2-methoxy-5-(2-ethylhexyloxy)-1,4-phenylenevinylene] (MEH-PPV) has attracted scientific attention because of its morphological and optical properties that enable its application in electroluminescent devices and solar cells, among others.[41−44] The combination of this material with organic or inorganic structures is a strategy to produce even more sophisticated devices, such as the transistors constructed by Aleshin[45] and other applications.[46−48]

Carbazole derivatives are also fascinating compounds because of their ability to generate charge-transfer complexes when associated with other electron carriers. Their polymerization has provided new and efficient compounds for application in electroluminescent devices and sensors.[49−55]

Considering these interesting compounds, the aim of this work was to produce distinct Phe−Phe self-assembled structures combined with electroluminescent compounds via supramolecular bottom-up methodologies and to determine the morphological and photophysical properties of the resulting materials. They were determined by steady-state and time-resolved fluorescence spectroscopy and scanning electron microscopy (SEM). The combined analysis of these results gives information on the delicate balance of forces that favor the formation of a specific structure in well-determined experimental conditions as well as on the charge-transfer complex formation between the luminescent additives and the peptide nanostructures, which are essential to evaluate their applications in solar cells.

RESULTS AND DISCUSSION

Self-assembled diphenylalanine (Phe−Phe) distinct structures were prepared in solvents with distinct polarizabilities and in the presence of luminescent additives with distinct electronic characteristics (electron donors and acceptors), solubility in distinct solvents (organic solvents and water), and electronic conjugation length (small molecules and polymers). All resulting self-assembled structures were numbered from Sm1 to Sm5 and the preparation conditions, used materials, and compounds as well as the details on the characterization methods and techniques are presented in Experimental Methods. They were studied by steady-state and time-resolved fluorescence spectroscopy along with SEM, and data obtained for each system (Sm1 to Sm5) are presented in the following subsections.

Sm1 Morphology and Photophysics—Self-Assembled Phe−Phe in Tetrahydrofuran. In Figure 1, SEM images of the Sm1 sample deposited on glass substrate are presented and they evidence lamellar structures of 2−10 μm wide, with shapes similar to the peony flowers-like, as those observed by Su et al.[56]

Steady-state fluorescence and excitation spectra obtained for Sm1 are shown in Figure 2. The excitation maximum wavelength is at 280 nm and the fluorescence maximum is at 325 nm, with a shoulder at 410 nm and both present low intensity, which is expected for Phe−Phe self-assembled structures.

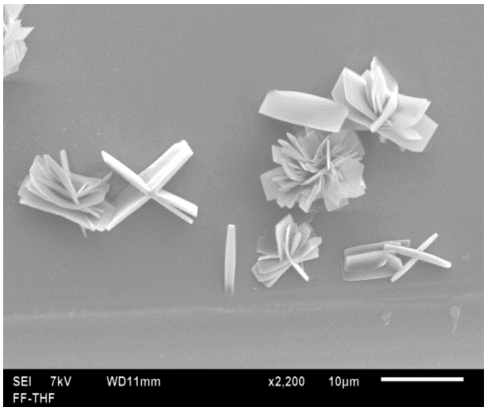

Figure 1. SEM images of the Sm1 sample, recorded at secondary electron imaging (SEI) with an electron beam energy of 7 kV, with a magnification of 2200 times.

Figure 3 presents the fluorescence decay curves recorded for Sm1 in the time-resolved emission spectroscopy (TRES) experiment, run as detailed in Experimental Methods, with excitation performed at 345 nm and fluorescence monitored at 360 (Figure 3A) and with excitation performed at 375 nm and fluorescence monitored at 400 and 420 nm (Figure 3B), according to the maxima excitation and emission wavelengths found in steady-state spectra presented in Figure 2. Table 1 presents the fluorescence lifetimes obtained from the multiexponential global fit of these decay curves, the pre-exponential factors, and the reduced χ^2 values that validate the exponential adjustments. It is observed that the decay curve recorded at 360 nm presents a biexponential behavior, whereas the decay curves recorded at 400 and 420 nm are triexponential. Although there are longer lifetimes, such as 8.8 ns for the biexponential curve and 4.8 ns for the triexponential curves, they contribute less than 10% to the total decay curves. On the other hand, the shorter lifetimes of tens of picoseconds obtained for the triexponential curves seem to be the most important contributions to these decays. However, they are too short to be accurately determined by the equipment used in these experiments because the NanoLed (pulsed led) used in the experiment presents a pulse width similar to those lifetimes (see equipment information in Experimental Methods). The lifetime of 1.2−1.8 ns that is observed in all decays is reliable and is in accordance with the lifetimes observed for Phe−Phe self-assembled structures.[57] Nevertheless, the multiexponential behavior observed for this sample is due to the fact that the self-assembling process originates a distribution of structures with distinct conjugation lengths, resulting in a distribution of electronic excited states that can be accessed by distinct excitation wavelengths.

According to the accepted Phe−Phe self-assembling mechanism, the lamellar structures shown in Figure 1 suggest the initial β-sheet structure formation, which, in THF, were unable to fold into themselves to generate nanotubes and, as shown by other authors, gave rise to other structures such as nanowires, vesicles, and gels.[58−62] Yet, the peony-flowers-like structures shown in Figure 1 are believed to result from lamellae stacking.[56] From Figure 2, the expected optical response for diphenylalanine assembles is obtained, which evidence Sm1 composition as being diphenylalanine only, although the fluorescence decay curves in Figure 3 reveal that

DOI: 10.1021/acsomega.8b02732
ACS Omega 2019, 4, 606−619

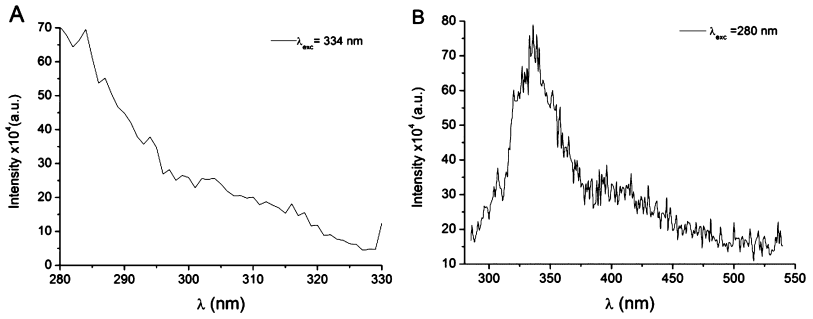

Figure 2. Steady-state spectra of (A) excitation (λ_{em} = 334 nm) and (B) fluorescence (λ_{exc} = 280 nm) recorded for Sm1.

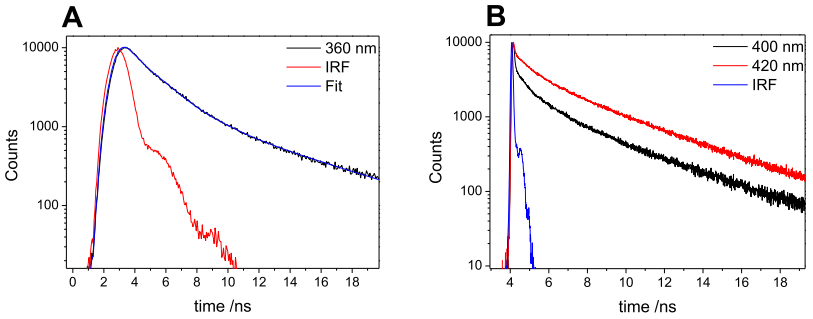

Figure 3. Fluorescence decay curves of Phe−Phe self-assembled structures in THF obtained (A) with excitation at 345 nm and emission monitored at 360 nm and (B) with excitation at 375 nm and emission monitored at 400 and 420 nm, with a time resolution of 4 ps/channel.

Table 1. Fluorescence Lifetimes and Pre-Exponential Parameters Obtained from the Multiexponential Adjustment of Fluorescence Decay Curves Recorded for Sm1

λ (nm)	360	400	420
A_1	0.9017	0.8378	0.9681
τ_1 (ns)	1.7076	0.0811	0.1370
A_2	0.0983	0.1023	0.0175
τ_2 (ns)	8.8089	1.2045	1.3529
A_3		0.0599	0.0144
τ_3 (ns)		4.8306	4.8834
χ^2	1.267	1.206	1.189

there is a distribution of structures with distinct conjugation lengths in Sm1.

Sm2 Morphology and Photophysics—Self-Assembled Phe−Phe with Additive MEH-PPV in THF. Figure 4 shows SEM images obtained for Sm2, in which sphere-like structures are observed. Because they have a sear aspect, it is inferred that these spheres may be vesicles. In fact, hollow structures are expected in Phe−Phe self-assembling.[63] According to Guo et al.,[63] Phe−Phe β-sheet bilayers fold into themselves to generate vesicles, in the same mechanism expected to occur here, or they fold into nanotubes, depending on preparation conditions. Considering it, interconversion between these structures may occur. This assumption is supported by the images shown in Figure 4C, which presents tubules, although in low occurrence.

Figure 5 shows fluorescence and excitation spectra obtained for the Sm2 sample. As shown in Figure 5A, the maximum of excitation is at 496 nm and a less intense band is observed at 330 nm, corresponding to the excitation maximum normally observed for MEH-PPV moieties and Phe−Phe structures, respectively. Figure 5B shows the emission spectra with excitation performed at these two excitation maxima. When excitation is performed at 496 nm, which is the characteristic excitation wavelength of MEH-PPV moieties, a fluorescence spectrum at the MEH-PPV general emissive region is recorded, with a maximum of fluorescence at 596 nm and a shoulder at 630 nm. A blue-shifted shoulder at 540 nm is also identified, which is related to MEH-PPV intrachain excitons.[64−66] Because it is of low intensity, it indicates that intrachain excitons are not the most important emission contribution in this system and aggregation is expected to occur to some extent. The red-shifted shoulder in the fluorescence spectrum at 630 nm is due to these aggregates. When excitation is carried out at 330 nm, emission occurs at the region in which

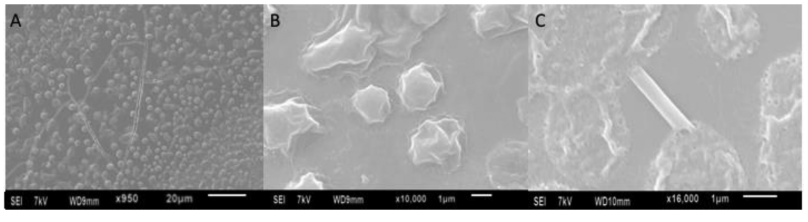

Figure 4. SEM images of Sm2, recorded at SEI with an electron beam energy of 7 kV, with a magnification of (A) 950, (B) 10 000, and (C) 16 000 times.

DOI: 10.1021/acsomega.8b02732
ACS Omega 2019, 4, 606−619

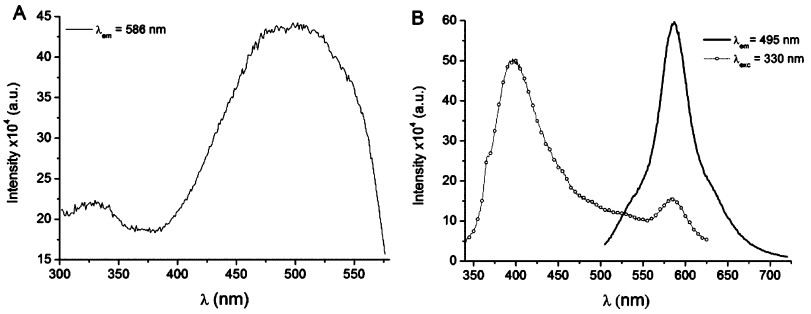

Figure 5. Steady-state spectra of (A) excitation (λ_{em} = 586 nm) and (B) fluorescence (λ_{exc} = 495 and 330 nm) recorded for Sm2.

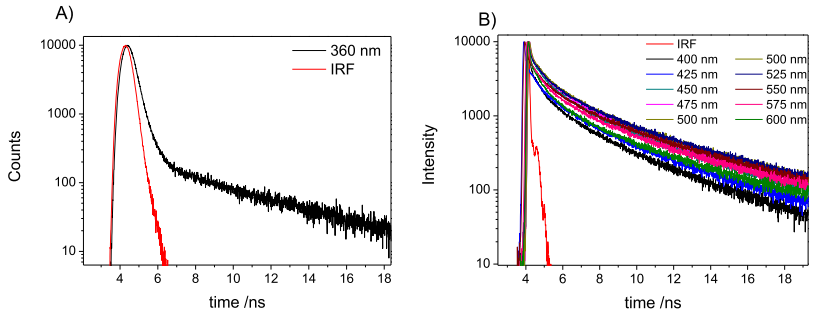

Figure 6. Fluorescence decay curves obtained for Sm2 with (A) excitation at 335 nm and fluorescence monitored at 360 nm and (B) excitation at 375 nm, with fluorescence monitored in the range of 400−600 nm, with a time resolution of 4 ps/channel.

Table 2. Fluorescence Lifetimes and Pre-Exponential Parameters Obtained from the Multiexponential Adjustment of Fluorescence Decay Curves Recorded for Sm2

λ (nm)	360	400	425	450	475	500	525	550	575	600
A_1	0.9874	0.6142	0.718	0.5758	0.5648	0.5244	0.6126	0.7695	0.7136	0.7442
τ_1 (ns)	0.2981	0.2768	0.3049	0.2027	0.2173	0.2768	0.2347	0.2369	0.2218	0.1630
A_2	0.0126	0.2695	0.2047	0.2952	0.2994	0.3250	0.2618	0.1632	0.2025	0.1846
τ_2 (ns)	5.5619	1.5891	1.6898	1.4975	1.5338	1.7159	1.5359	1.5355	1.4798	1.2735
A_3		0.1164	0.0773	0.1289	0.1358	0.1506	0.1257	0.0673	0.0839	0.0712
τ_3 (ns)		5.2246	5.7523	5.7893	6.0544	6.4745	6.2725	6.3536	6.2374	5.8809
χ^2	1.089	1.112	1.151	1.193	1.160	1.120	1.134	1.116	1.241	1.157

MEH-PPV fluorescence is usually observed, although of low intensity (see Figure S1 in the Supporting Information). In addition, a more intense fluorescence band at 410 nm is observed, and it is coincident with the maximum of fluorescence observed for Sm1, composed only of Phe−Phe self-assembled structures.

The formation of vesicle-like structures interconnected by nanotubes in Sm2 enables us to infer on their mechanism of formation, once it is our argument that vesicles form because of a more important polymer−peptide interaction over a less important peptide−peptide π-stacking interaction, showing that the self-assembling is governed by a dispute of distinct interaction forces. Also, because by fluorescence spectroscopy excitation at the wavelength of 330 nm results in a mixed emission spectrum containing elements from both MEH-PPV moieties and Phe−Phe structures, it is expected that hopping (and, therefore, charge transfer) processes occur in such a system. Comparing the fluorescence spectra of the MEH-PPV solution in THF (10^{-6} g L^{-1}) (see Figure S1 in the Supporting Information) to those obtained for Sm2 (Figure 5), it is noteworthy that the most prominent emission occurs at the characteristic region of MEH-PPV moieties. Nevertheless, the relative intensity of fluorescence peaks at 550 nm, related to MEH-PPV intrachain aggregates, and 630 nm, related to the emission of interchain aggregates (I_{550nm}/I_{630nm}), is very distinct, being 3 for Sm2 and 0.5 for the MEH-PPV solution. This evidences that emission from the intrachain aggregates is more important in the peptide/MEH-PPV system than in the MEH-PPV solution. Although it was expected that in Sm2, MEH-PPV chain aggregation would be more important than in solution, this result is evidence for a nonexpected degree of disaggregation of MEH-PPV when in contact with peptide structures, favored by π-stacking interactions between them, possibly leading to the formation of a charge-transfer complex. This assumption can be properly exploited by time-resolved fluorescence spectroscopy.

Fluorescence decay curves obtained by the TRES experiment executed for the Sm2 sample are presented in Figure 6, and fluorescence lifetimes obtained from the multiexponential fit of these curves are presented in Table 2. For the TRES experiment of all samples presented in this work, excitation and emission wavelengths to monitor fluorescence decays were selected based on the steady-state spectra for all samples. Detailed information is in the Experimental Methods section. Figure 6A presents the fluorescence decay curve recorded with excitation at 335 nm and fluorescence monitored at 360 nm, which shows a biexponential behavior, because at this wavelength, only Phe−Phe structure is emitting, nevertheless,

DOI: 10.1021/acsomega.8b02732
ACS Omega 2019, 4, 606−619

with a shorter lifetime, when compared to that of Sm1. As longer emission wavelengths are analyzed, the decay curves become multiexponential, indicating the increasing contribution of MEH-PPV to the total decay curve. In fact, the decay curves recorded with excitation at 375 nm and emission monitored at the 400−600 nm range present at least three lifetimes, 0.3, 1.6, and 6 ns. Comparing these lifetimes to those obtained for Sm1, the shorter lifetimes are the most prominent in both samples. They present a longer lifetime, around 6 ns with very low contribution to the total decay curve. Nevertheless, the Sm2 sample presents a third lifetime, around 1.5 ns, contributing 15−20% to the total curve that is very close to the lifetime found for the MEH-PPV solution used as the additive (see Figure S2 in the Supporting Information). It is noteworthy that at the 425−500 nm emission range, there is a change in the value of the intermediary lifetime, as well as on its contribution. It becomes slightly longer, being 1.7 ns, with around 30% contribution. Also, the longer lifetime becomes more important at this emission region, contributing 15% of the total decay curve. This behavior change may be related to an energy-transfer complex formation in this system, active at this emission region.

Sm3 Morphology and Photophysics—Self-Assembled Phe−Phe with Additive 9-Vinyl-carbazole in THF. To explore the doping effect on the Phe−Phe self-assembling and infer on the charge-transfer complex formation, the sample Sm3 was prepared using 9-vinyl-carbazole (9Cz) as the fluorescent additive. Compared to MEH-PPV, it is a small molecule (M_w = 193.24 g mol^{-1}; volume = 614.60 Å^3; surface area = 285.74 Å^2) and an electron acceptor, whereas MEH-PPV is an electron donor. These distinct characteristics may have distinct influence on the driving forces of the peptide self-assembling, favoring, in certain conditions, electrostatic interactions, in other conditions, $\pi-\pi$ stacking interactions. Samples were prepared as described in the Experimental Methods, and SEM images obtained to evidence their morphologies are presented in Figure 7.

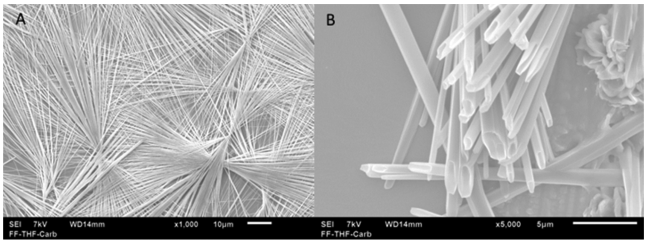

Figure 7. SEM images obtained for the sample Sm3, recorded at SEI with an electron beam energy of 7 kV, with a magnification of (A) 1000 times and (B) 5000 times.

Figure 7 shows nanotubes resulting from Phe−Phe self-assembling with carbazole as the additive. When deposited on a glass substrate, nanotubes grew radially from a growth seed that is formed while the solvent is still present in the substrate. After solvent evaporation and with the impingement of two nanotubes, its growth is interrupted. From Figure 7B, the hexagonal geometry of the Phe−Phe nanotubes is observed, as expected[33] in conditions where electrostatic interactions in the inner part of the nanotubes are favored, for instance, when water is the solvent. In a previous work,[44] we showed that water is inserted in the prime Phe−Phe nanotubes to result in the hexagonal geometry via electrostatic interactions between the carboxyl and amino end-groups of the peptide with water molecules. In these systems, however, water is not present, even though hexagonal geometry is observed. Yet, the same lamellar structures observed in Sm1 are also observed here, although in an extremely low proportion. Information on the balance of interactions can be obtained by steady-state fluorescence spectroscopy because they can influence carbazole fluorescence and excitation spectra. They are presented in Figure 8.

Emission spectra were recorded upon distinct excitation wavelengths, 350, 366, and 381 nm, corresponding to the maxima wavelengths observed in the steady-state excitation spectra. When compared to the spectra expected for 9Cz diluted solutions in good solvents, such as chloroform[67] and THF,[68] these are structureless and red-shifted, with its maximum of around 415 nm (2.99 eV), whereas the fluorescence maximum for the isolated carbazole is expected to occur at 380 nm (3.26 eV),[67] which corresponds to a loss of energy upon nonradiative deactivation of 0.27 eV. The broad excitation spectrum suggests the formation of ground-state aggregates in this sample. Also, there is a fluorescence red shift upon excitation at longer wavelengths and a shoulder of low intensity in the 530−580 nm region, indicating excimer formation. These findings suggest that carbazole moieties are distributed along the nanotubes in a short distance from each other and, considering the possible electrostatic interaction between carbazole moieties and peptide units, this proximity may inform about the self-assembling mechanism.

Taking SEM results for Sm3 into account (Figure 7), where we identified hexagonal nanotubes with low occurrence of lamellar structures, we infer that these lamellae are acting as growth seeds for nanotubes obtained with carbazole. Interactions between Phe−Phe and carbazole moieties may influence the π-stacking interaction, guaranteeing the self-assembling into nanotubes, whereas when 9Cz is absent, the balance of interaction forces prioritizes electrostatic forces upon π-stacking, resulting in lamellae and vesicles. Because of 9Cz characteristic of electron acceptance, its smaller

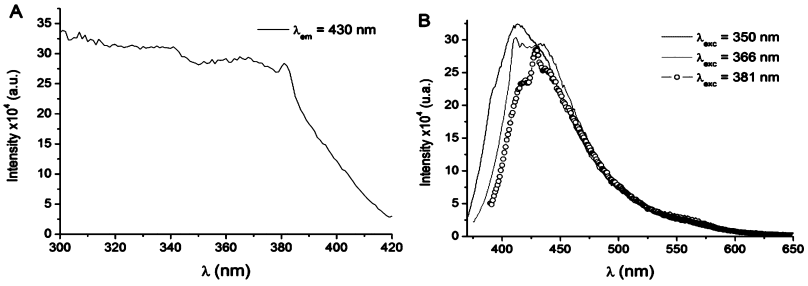

Figure 8. Steady-state spectra of (A) excitation (λ_{em} = 430 nm) and (B) fluorescence (λ_{exc} = 350, 366, and 381 nm) recorded for Sm3.

DOI: 10.1021/acsomega.8b02732
ACS Omega 2019, 4, 606−619

dimensions compared to those of MEH-PPV, and the luminescent characteristics recorded for Sm3, that is, excitation-dependent fluorescence and excimer occurrence (Figure 8B), it is possible to locate the carbazole moieties distributed along the nanotubes and interacting with it via π-stacking. In this condition, 9Cz favors $\pi-\pi$ stacking to subdue electrostatic interactions and, consequently, favors nanotube formation over vesicles. Also, because a comparison between the fluorescence spectra of 9Cz diluted solutions and Sm3 evidences loss of energy upon deactivation of 0.27 eV, it may refer to specific carbazole−nanotube interactions, resulting in a charge-transfer complex that may be formed in Sm3. Considering this possibility, the fluorescence lifetime can inform about the occurrence of such interactions and the formation of energy-transfer electronic excited-state complexes because it may affect the fluorescence decay curves expected for both the additive and the dipeptide structure. Figure 9 presents the fluorescence decay curves recorded for Sm3, and Table 3 presents the corresponding fluorescence lifetimes.

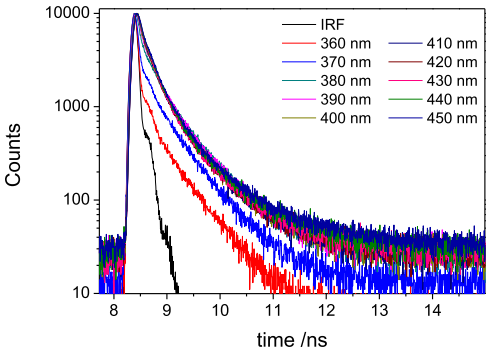

Figure 9. Fluorescence decay curves recorded for Sm3 with excitation at 345 nm and emission monitored at the range of 360−450 nm, with a time resolution of 3.7 ps/channel.

From Figure 9, it is noteworthy that the decay curve shapes change as the fluorescence is monitored at longer wavelengths. With emission monitored at 360 and 370 nm, the decay curve is biexponential, presenting a shorter lifetime of 1.6 ns and a longer lifetime of 5.6 ns, corresponding to the lifetimes of the Phe−Phe structure. At longer emission wavelengths, the decay curves are fitted by a multiexponential function, giving rise to the same lifetimes observed earlier and a third component of 2−3 ns, contributing 20−25% to the total decay curve. As the fluorescence is monitored at longer wavelengths, it is observed that the shorter lifetime assumes values of around 1.0−1.2 ns, being longer than the observed when the fluorescence is monitored at shorter emission wavelengths, whereas the longer lifetime assumes values of 7−8 ns. In this emission region, it is expected that the decay curve has more substantial contributions of the 9Cz additive; nevertheless, these longer lifetimes are shorter that those of the 9Cz solution, which is expected to be around 14 ns (see Figure S3 in the Supporting Information). On the other hand, the shorter lifetimes of Sm3 are longer than those obtained for 9Cz. Thus, the Sm3 fluorescence lifetimes are distinct from those of the individual components, indicating that a complex is formed to stabilize the electronic excited states of shorter lifetimes and destabilize the longer-lived excited states, which may alter the population of triplet states of 9CZ, which is a phosphorescent molecule.

Sm4 Morphology and Photophysics—Self-Assembled Phe−Phe with Additive MPS-PPV in Water. Figure 10 shows Phe−Phe nanostructures self-assembled in water and doped with poly[5-methoxy-2-(3-sulfopropoxy)-1,4-phenylenevinylene] (MPS-PPV), the PPV water-soluble derivative, similar in structure to MEH-PPV (with a sulfonic termination instead of a long ether substituent, as shown in Figure 18D, Experimental Methods), which were assigned as Sm4. Nanotubes of a hexagonal structure were obtained under these conditions, in contrast with vesicles obtained when THF is the solvent and MEH-PPV is the additive. From Figure 10, the nanotube growth occurs radially in a seeded growth regime and they associate with each other to generate microtubes. It is evident that although these samples are prepared with an additive very similar to MEH-PPV, no vesicles are formed, only nanotubes, which evidence a preferable π-stacking of the diphenylalanine aromatic rings driven by the Coulombic interaction between the Phe−Phe carboxyl and amino end-groups and water.

Figure 11 shows excitation and fluorescence spectra obtained for these samples. The fluorescence spectra of MPS-PPV solutions (Figure 11C) are observed in a region similar to those obtained for MEH-PPV solutions (see Figure S1 in the Supporting Information), presenting its maximum at 530 nm, a shoulder at 470 nm, and another one of low intensity at 415 nm. Its excitation spectrum (Figure 11A) is peculiar and presents a maximum at 370 nm, with a shoulder at 430 nm and a half-intensity peak at 485 nm. These spectral characteristics ensure that electronic states involved in the photophysical processes identified for these systems are very similar to those identified for systems containing MEH-PPV as the additive, enabling a comparison between Sm2 and Sm4 in terms of behavior and possible interactions, fostering considerations on charge-transfer processes and complex formation.

The sample Sm4 was produced to evaluate the modulation of the Phe−Phe/polymer system photophysical and/or morphological behavior, considering that nanotubes are expected to form in water and vesicles were obtained in

Table 3. Fluorescence Lifetimes and Pre-Exponential Parameters Obtained from the Multiexponential Adjustment of Fluorescence Decay Curves Recorded for Sm3

λ (nm)	360	370	380	390	400	410	420	430	440	450
A_1	0.3789	0.5966	0.7883	0.8543	0.7463	0.7541	0.7026	0.7435	0.7026	0.7161
τ_1 (ns)	1.8225	1.4099	0.5764	0.5033	0.8957	0.6980	0.9577	1.0973	1.0800	1.2793
A_2	0.6211	0.4034	0.1165	0.1029	0.1929	0.2001	0.2440	0.2097	0.2483	0.2212
τ_2 (ns)	5.7657	5.6375	2.1674	2.1934	2.7336	2.3171	2.6383	2.8991	2.6206	3.2501
A_3			0.0951	0.0427	0.0607	0.0458	0.0535	0.0468	0.0491	0.0627
τ_3 (ns)			5.8746	6.1348	6.9160	6.7946	7.4448	7.8635	7.7008	8.1387
χ^2	1.143	1.226	1.177	1.236	1.107	1.178	1.110	1.141	1.164	1.157

DOI: 10.1021/acsomega.8b02732
ACS Omega 2019, 4, 606−619

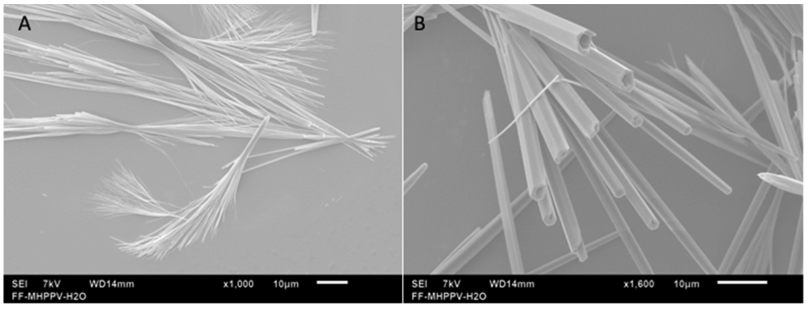

Figure 10. SEM images obtained for the Sm4 sample, recorded at SEI with an electron beam energy of 7 kV, with a magnification of (A) 1000 and (B) 1600 times.

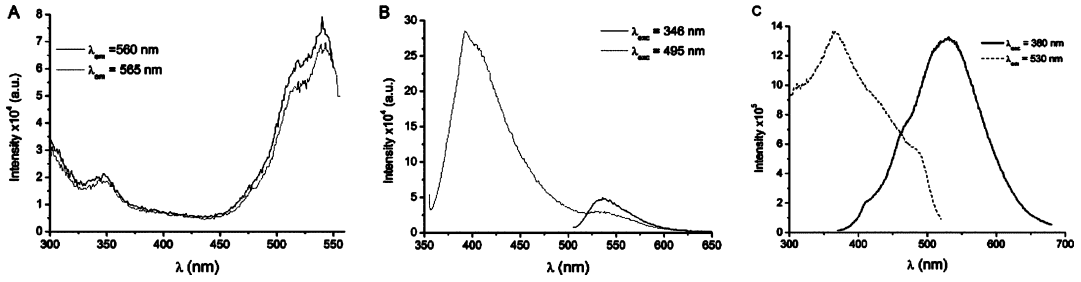

Figure 11. Steady-state (A) excitation (λ_{em} = 560 and 565 nm) and (B) fluorescence (λ_{ecx} = 346 and 495 nm) spectra obtained for the Sm4 sample and (C) excitation (λ_{em} = 530 nm) and fluorescence (λ_{exc} = 360 nm) spectra of MPS-PPV 10^{-4} g L^{-1} solution in water.

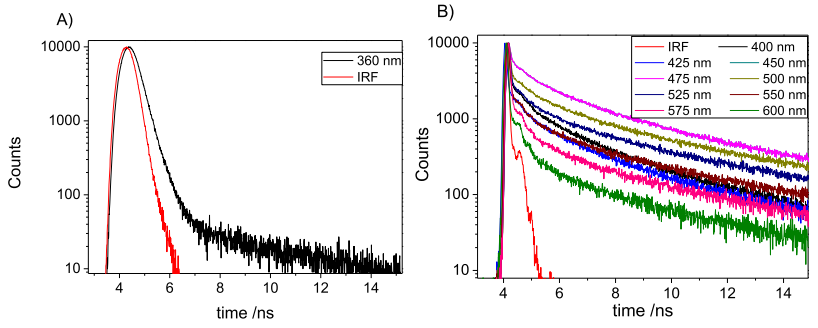

Figure 12. Fluorescence decay curves recorded for Sm4 (A) with excitation performed at 345 nm and fluorescence monitored at 360 nm and (B) with excitation performed at 375 nm and fluorescence monitored at the range of 400−600 nm, with a time resolution of 3.7 ps/channel.

Table 4. Fluorescence Lifetimes and Pre-Exponential Parameters Obtained from the Multiexponential Adjustment of Fluorescence Decay Curves Recorded for Sm4

λ (nm)	360	400	425	450	475	500	525	550	575	600
A_1	0.9970	0.8782	0.5474	0.6934	0.5449	0.748	0.8663	0.8696	0.9845	0.9782
τ_1 (ns)	0.2788	0.0658	0.3500	0.1754	0.1738	0.0817	0.0531	0.0555	0.0307	0.0361
A_2	0.0030	0.0902	0.3397	0.2151	0.3085	0.165	0.0857	0.0838	0.0105	0.0152
τ_2 (ns)	5.3119	1.2191	1.8151	1.5787	1.6586	1.5344	1.387	1.3199	1.0772	1.2531
A_3		0.0316	0.1128	0.0915	0.1467	0.0869	0.0479	0.0466	0.005	0.0067
τ_3 (ns)		4.8778	5.8992	5.8118	6.4197	6.5891	6.6182	6.5259	6.1931	6.4409
χ^2	1.150	1.095	1.12	1.121	1.072	1.18	1.128	1.087	1.023	1.096

THF (Figures 10 and 4, respectively). Once nanostructures are obtained, the role of PPV derivatives in the complex formation and properties is elucidated. Figure 11A,B shows Sm4 fluorescence and excitation spectra, which are compared to those obtained for Sm2 (Figure 5). From Figure 11B, when excitation of Sm4 is performed at 330−350 nm, an emission band at 400 nm is observed, as for Sm2. Excitation at 495 nm results in a fluorescence maximum at 540 nm, which is blue-shifted with respect to that identified for Sm2 but red-shifted in comparison to the fluorescence spectra of the MPS-PPV solution employed to produce the Sm4 sample, indicating MPS-PPV aggregation in the system. Also, the shoulders identified in the fluorescence spectra of the MPS-PPV solution are not present in Sm4, indicating that aggregated chains are responsible for the most prominent fluorescence rather than intrachain excitons that might exist in Sm4. In addition, as also observed for Sm2, fluorescence at 540 nm is also observed when excitation is carried out at 340 nm, indicating that a charge-transfer complex is formed in this sample, which can be characterized by time-resolved fluorescence spectroscopy.

DOI: 10.1021/acsomega.8b02732
ACS Omega 2019, 4, 606−619

Figure 12 presents the decay curve recorded for Sm4, and lifetimes are presented in Table 4. The decay curve in Figure 12A is biexponential, with a shorter lifetime of around 300 ps with over 90% contribution. The longer lifetime, which is greater than 5 ns, contributes less than 3% to the total decay curve. As the fluorescence is monitored at longer wavelengths, a third component of 1.2−1.5 ns rises, with 8−10% contribution. The shorter lifetime is diminished from 300 to 30 ps from shorter to longer emission wavelengths, with 85−97% contribution. The longer lifetime presents variable contributions as the monitored emission wavelength changes and assumes longer values of 5.8−6.5 ns. At the emission region from 425 to 500 nm, its contribution is around 11−14%, whereas from 520 to 600 nm, its contribution drops to 0.5%. A behavior change is also observed at the region of emission from 425 to 500 nm, where the intermediary lifetime becomes slightly longer, assuming values of around 1.5−1.8 ns, but contributes almost 30% to the total decay curve. This behavior is similar to that observed for Sm2.

Sm5 Morphology and Photophysics—Self-Assembled Phe−Phe with Additive PVK. Figure 13 presents the SEM images registered for Sm5, where nanotubes were observed, also with the radial growth.

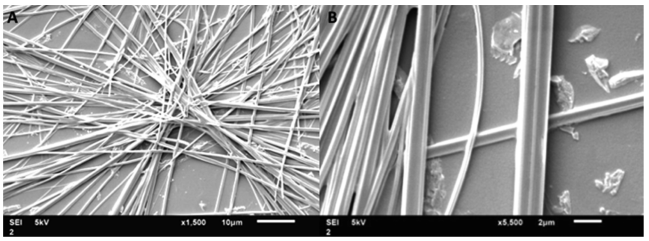

Figure 13. SEM images obtained for the Sm5 sample, recorded at SEI with an electron beam energy of 7 kV, with a magnification of (A) 1500 and (B) 5500 times.

Because THF was the solvent, vesicles were expected to form in Sm5, as occurred in Sm2, if the solvent had a predominant effect on the Phe−Phe self-assembling. Because only nanotubes were formed, it shows that the effect of the solvent on self-assembling is not as pronounced as the inductive effect of the carbazole units.

Fluorescence and excitation spectra obtained for Sm5 samples are presented in Figure 14. Excitation spectra were recorded with the emission monitored at 426 and 547 nm and fluorescence spectra were recoded with excitation at 265, 272, 294, 351, 364, and 526 nm, which were selected from the excitation spectra.

Excitation spectra monitored at these two distinct emission wavelengths are also distinct. When emission is monitored at 426 nm, the maximum of excitation is at 351 nm. With the fluorescence monitored at 547 nm, a broad band with a maximum at 366 nm and two other important peaks at 273 and 298 nm are observed. This shows that there are distinct emitting moieties in this system.

Both steady-state excitation and emission spectra recorded for Sm5 are distinct of the spectra normally obtained for PVK solution that originated Sm5 (see Figure S4 in the Supporting Information). Fluorescence spectra recorded at distinct excitation wavelengths occur in distinct regions, evidencing their excitation wavelength-dependent behavior. When excitation is performed at 265 and 272 nm, an intense fluorescence is observed at 300−330 nm and a less intense band is observed at 450 nm. With excitation at 294 nm, a band at 350 nm occurs in comparable intensity of a band in 450 nm. When excitation is performed at 351 and 364 nm, a similar band at 450 is observed, and excitation performed at 526 nm resulted in fluorescence at 580 nm. This also evidences the coexistence of distinct fluorescent moieties in Sm5, which is due to charge-transfer complex formation and it can be exploited by time-resolved fluorescence. Yet, excitation and fluorescence spectra are overlapped, which can result in important self-absorption effects.

Figure 15 presents the fluorescence decay curves recorded for Sm5, and Table 5 summarizes the data obtained from the multiexponential fit of these curves.

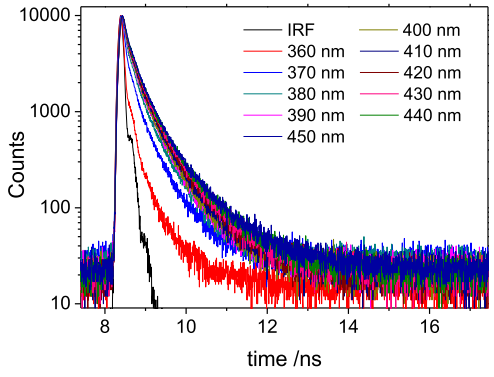

Figure 15. Fluorescence decay curves recorded for Sm5, with excitation at 345 nm and emission monitored from 360 to 450 nm, with a time resolution of 4.2 ps/channel.

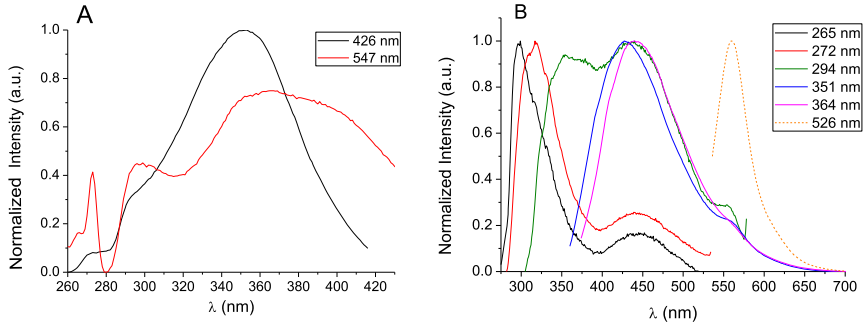

Figure 14. Normalized (A) excitation (λ_{em} = 426 and 547 nm) and (B) fluorescence (λ_{exc} = 266, 272, 294, 351, 364, and 526 nm) spectra obtained for the Sm5 sample.

DOI: 10.1021/acsomega.8b02732
ACS Omega 2019, 4, 606−619

Table 5. Fluorescence Lifetimes and Pre-Exponential Parameters Obtained from the Multiexponential Fit of Fluorescence Decay Curves Recorded for Sm5

λ (nm)	360	370	380	390	400	410	420	430	440	450
A_1	0.9622	0.9635	0.9312	0.9207	0.9065	0.9016	0.9007	0.8960	0.8799	0.8707
τ_1 (ns)	1.0797	1.0263	1.2644	1.2843	1.4012	1.4499	1.4078	1.6709	1.6248	1.6114
A_2	0.0378	0.0365	0.0688	0.0793	0.0935	0.0984	0.0993	0.1040	0.1201	0.1288
τ_2 (ns)	4.8947	4.7613	5.1388	5.2224	5.4054	5.5682	5.5288	6.1332	6.1066	6.0821
χ^2	1.177	1.150	1.131	1.124	1.186	1.261	1.285	1.262	1.269	1.261

Table 6. HOMO−LUMO Band Gaps (eV) Calculated for the Phe−Phe Trimer in Neutral and Zwitterion Forms in Vacuum, THF, and Water

solvent	vacuum		THF		water	
trimer form	neutral	zwitterion	neutral	zwitterion	neutral	zwitterion
bandgap (eV)	4.131	4.089	4.174	3.990	4.210	3.992

The decays showed a biexponential behavior, with a shorter lifetime varying from 1 to 1.6 ns toward longer emission wavelengths and contributing 87−96% to the total decay curve. The longer lifetime varies from 4.8 to 6.1 ns as monitored at longer emission wavelengths, and it contributes 3−12% to the total decay curve.

This behavior is distinct from that observed for pure poly(vinyl carbazole) (PVK), which showed a multiexponential behavior (see Table S3 and Figure S5 in the Supporting Information) and is related to the disaggregation of the polymer backbones and its interaction with the Phe−Phe structure. Comparing it to the Sm1 behavior, τ_1 are very similar in value and contribution; nevertheless, Sm1 behavior is also multiexponential (see Table 1). It is clear that the biexponential behavior of Sm5 and its fluorescence lifetimes reflect the formation of new electronic excited states, originated from the Phe−Phe/PVK interaction, which resulted in a new structure, with a distinct photophysical behavior from the initial compounds.

Theoretical Calculations. To understand the reasons for the balance of interactions of distinct Phe−Phe formed upon distinct solvent and additives, theoretical calculations were performed to give information on the energies of highest occupied molecular orbital (HOMO) and lowest unoccupied molecular orbital (LUMO) orbitals and band gaps of a trimer of Phe−Phe in neutral and zwitterion forms in vacuum, tetrahydrofuran (THF), and water. The trimer was used because it represents the basic interacting structure on self-assembled structures of Phe−Phe.[69]

From the optimized results of the structures, it is possible to infer that components in the zwitterion are closer to one another than the neutral components at any solvent used. This greater proximity is due to more effective interaction between carboxyl end-groups in the zwitterion peptide. Calculated energy band gaps are shown in Table 6.

It is noteworthy that the band gap for neutral forms is always slightly higher than the band gap of the corresponding zwitterion. Also, the band gap of the neutral form is larger in solvents than in vacuum, being large in water, whereas zwitterion is equally stabilized in both solvents because of the electrostatic interactions between amino and carboxyl end-groups of the peptide that become important in solvents and that give rise to interactions between the peptide and the solvent molecules.

In Figures 16 and 17 are shown HOMO and LUMO orbitals for the neutral structures of the Phe−Phe trimer in vacuum, THF, and water. In Figure 16, HOMO orbitals are localized on the amide linkage and carboxyl end-groups of the peptide structure, whereas LUMO orbitals are widely spread on the aromatic rings and, in solvents, they are more delocalized over the trimer than in vacuum.

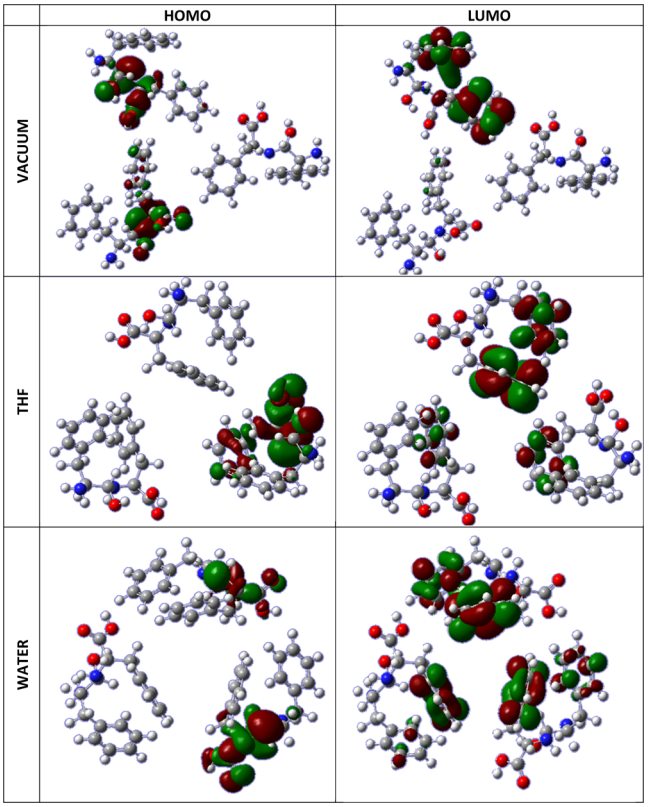

Figure 16. Representation of the HOMO and LUMO orbitals for the neutral Phe−Phe trimer in vacuum, THF, and water.

Figure 17 presents the HOMO and LUMO orbitals calculated for the zwitterion Phe−Phe trimer. Similar to the neutral structure, the zwitterion HOMO is localized on the amide linkage for the trimer in vacuum and THF. In water, on the other hand, it is localized over an aromatic ring of a diphenylalanine molecule. LUMO orbitals are on the aromatic rings and delocalized on the trimer. The distinct delocalization is the reason for the larger band gaps of zwitterion when compared to the band gaps of neutral structures. LUMO orbitals are very similar in water and THF. As expected, the HOMO and LUMO of zwitterion structures are more delocalized over the trimer than the neutral structure. It is

DOI: 10.1021/acsomega.8b02732
ACS Omega 2019, 4, 606−619

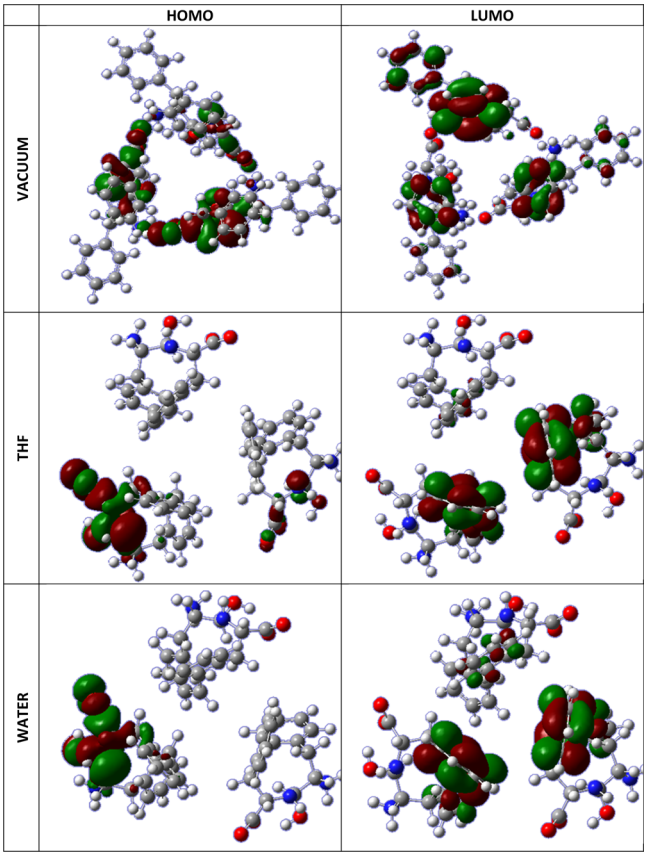

Figure 17. Representation of the HOMO and LUMO orbitals for the zwitterion Phe−Phe trimer in vacuum, THF, and water.

noteworthy that LUMO and HOMO orbitals are π-shaped in neutral and zwitterion forms.

Because of this orbital delocalization, distinct interactions with the additives are possible, depending on the additive electronic properties. MEH-PPV (as well as MPS-PPV) is an electron donor, whereas carbazole derivatives are electron acceptors; thus, they interact differently with the peptide, giving rise to distinct self-assembled structures. Therefore, π-stacking interactions between Phe−Phe aromatic rings and the MEH-PPV backbone are favored in THF, where Phe−Phe is in the neutral form, originating in a β-pleated sheet structure with an interleaved polymer that stacks in lamellae and results in a vesicle or sphere. On the other hand, with carbazole derivatives, preferable interactions are electrostatic between the end-groups of the peptide and the nitrogen atom of the carbazole structure. This is an acceptable explanation in either neutral or zwitterion form, based on the delocalization of the HOMO orbital on the carboxyl and amino groups of the peptide. Therefore, this interaction is preferable in water as well as in THF. As a consequence, aromatic rings of the peptide can interact with each other in a π-stacking-type interaction, and this is the initial step for the peptide self-assembling into a nanotube. In this way, nanotubes are formed when carbazole is the additive, even when the solvent is THF. Yet, when in water, because of the strong hydrogen bonds that are formed with the charged end-groups of the peptide in the zwitterion or with the dipoles in the neutral structure, the interaction with solvents directs the self-assembling rather than the interaction with the additive MPS-PPV, which is not the driving force to the self-assembling anymore, and nanotubes are obtained.

CONCLUSIONS

This work corroborates that Phe−Phe self-assembling is governed by preparation conditions and, thus, can be controlled. Additives with distinct characteristics such as electron donor/acceptors or polymeric/small conjugated molecules interfere in the nanostructure mechanism of formation, resulting in distinct structures, showing that the self-assembling process is driven by the influence each additive exerts on the dominant interaction forces. In solvent THF, MEH-PPV moieties favor vesicle formation, whereas when the additive is a carbazole derivative, nanotubes are obtained. On the other hand, when water is the solvent, nanotubes are obtained even when MPS-PPV (a water-soluble derivative similar, in structure, to MEH-PPV) is the additive. This result reinforces that water exerts a dominant influence on Phe−Phe self-assembling through electrostatic interactions with the amino and carboxyl end-groups of the peptide, favoring the aromatic ring π-stacking interactions between Phe−Phe molecules, in such a way that only hexagonal nanotubes are generated. These conclusions are corroborated by the computational simulations in which Phe−Phe zwitterion HOMO and LUMO are more delocalized in solvents and present shorter band gaps, suggesting that the self-assembling is initially driven by trimers through electrostatic interactions that orient the second step involving π-stacking interactions.

With regard to the fluorescence spectral characteristics of each system, they are distinct from their precursors. The influence of molecular weight was evaluated by comparing the morphologies of systems produced with 9Cz and PVK. It is noteworthy that only nanotubes were obtained, revealing that the dominant interaction with the peptide is related to the electron acceptor characteristic rather than the chain length. Yet, their steady-state and time-resolved fluorescent responses evidence the charge-transfer complex formation between the additive and the self-assembled peptide. Excitation and fluorescence spectra of Sm3 and Sm5 are distinct of 9Cz and PVK, showing the influence of Phe−Phe in the electronic excited states. Yet, Sm3 showed a broad and excitation wavelength-dependent fluorescence, which is also indicative of a charge-transfer complex.

Fluorescence lifetimes recorded for Sm3 evidenced a distinct dynamic behavior, compared to the individual components, because of the complex formation, which occurs to stabilize the electronic excited states of shorter lifetimes and destabilize the longer-lived excited states. It is related to an alteration of the population of triplet states of 9Cz when it is part of the complex with Phe−Phe. On the other hand, fluorescence lifetimes of Sm5 resulted in a biexponential behavior, which is the evidence for the Phe−Phe/PVK interaction in a complex.

Steady-state fluorescence spectra of systems Sm2 and Sm4 are also peculiar and distinct of those recorded for the individual components. Excitation upon shorter wavelengths produces, along with more energetic luminescence, emission in the characteristic region of MEH-PPV (or MPS-PPV) moieties, although of low intensity. This mixed emission spectrum suggests that a hopping process occurs and, therefore, the charge-transfer complex formation between the polymer and the peptide structure occurs in a nanotube or vesicle-like form. Fluorescence lifetimes measurements evidenced electronic excited states more stabilized in Sm2 and

DOI: 10.1021/acsomega.8b02732
ACS Omega 2019, 4, 606−619

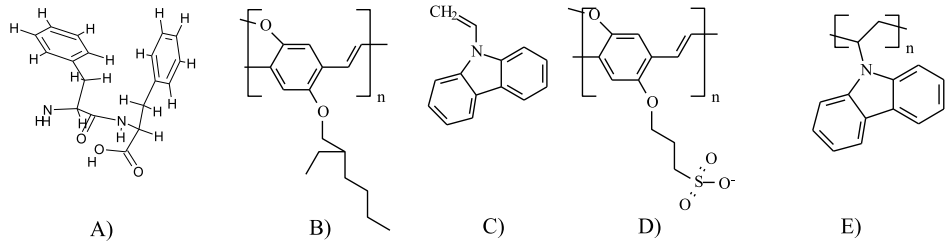

Figure 18. Chemical structures of (A) Phe−Phe, (B) MEH-PPV, (C) 9Cz, (D) MPS-PPV, and (E) PVK.

Sm4 than in MEH-PPV or MPS-PPV alone, which evidences the complex formation.

It is a breakthrough of this work that these results show that Phe−Phe nanotubes can be generated in organic solvent, taking advantage of their ability to interconvert, avoiding humidity in the inner part of the nanotube, which is undesired in photovoltaic devices. Also, Phe−Phe combination with luminescent compounds results in new materials with unique photophysical properties that can be widely exploited in this application field.

EXPERIMENTAL METHODS

Sample Preparation. Phe−Phe (Sigma-Aldrich) was self-assembled in a liquid phase, in an Eppendorf flask, from a mixture of its solution in 1,1,1,3,3,3-hexafluoro-2-propanol (HFP) (Aldrich) with the additive solution prepared in the adequate solvent. Detailed preparation protocols are presented below, and chemical structures are presented in Figure 18.

9-Vinyl-9*H*-carbazole solution in THF: (1.95 ± 0.01) mg of 9Cz, M_w = 193.244 g mol^{-1} (98% pure, Sigma-Aldrich), was dissolved in 10 mL of THF (Tedia, spectroscopic grade) to produce a 10^{-4} mol L^{-1} solution, which was, then, diluted to 10^{-6} mol L^{-1}.

MEH-PPV-MEH-PPV in THF: (2.20 ± 0.01) mg of MEH-PPV, M_w = 125 000 Da, M_n/M_w = 5 (Sigma-Aldrich) was dissolved in 10 mL of THF (Tedia, spectroscopic grade) to produce 10^{-2} g L^{-1} solution.

Poly(9Cz)—PVK in THF: (1.68 ± 0.01) mg of poly(9Cz) (PVK), M_n = 25 000−50 000 g mol^{-1}, and M_n/M_w = 2 (Sigma-Aldrich) was dissolved in 10 mL of THF (Tedia, spectroscopic grade), and a 10^{-2} g L^{-1} solution was obtained.

System Sm1—Phe−Phe structures produced in THF: (0.53 ± 0.01) mg of Phe−Phe was dissolved in 200 μL of HFP (Aldrich) in an Eppendorf flask, and 10 μL of this solution was placed over a glass substrate together with 10 μL of THF. The glass substrate was placed in an oven at 45 °C for 30 min to promote the solvent removal, and it was sealed and stored at 6 °C. Simultaneously, 200 μL of THF was placed in an Eppendorf flask initially containing the Phe−Phe solution, and it was also stored under refrigeration.

System Sm2—Phe−Phe structures produced in THF with MEH-PPV as the additive: (0.55 ± 0.01) mg of Phe−Phe was dissolved in 200 μL of HFP in an Eppendorf flask. A 10 μL aliquot of this solution was placed over a glass substrate, and immediately, the same volume of the MEH-PPV solution previously prepared was added to it. This glass substrate was also placed in an oven at 45 °C for 30 min for solvent removal and stored at 6 °C. Also, 200 μL of the MEH-PPV solution was placed in an Eppendorf flask containing the Phe−Phe solution and stored at 6 °C.

System Sm3—Phe−Phe structures produced in THF with 9-vinyl-9*H*-carbazole as the additive: (0.52 ± 0.01) mg of Phe−Phe was dissolved in 200 μL of HFP. A 10 μL aliquot of this solution was placed over a glass substrate with another 10 μL of 9-vinyl-9*H*-carbazole solution. The solvent was removed, and the substrate was stored. Also, 200 μL of the 9Cz solution was placed in an Eppendorf flask containing the Phe−Phe solution, and it was stored at 6 °C.

System Sm4—Phe−Phe structures produced in water and MPS-PPV as the additive: the mass of (0.55 ± 0.01) mg of Phe−Phe was dissolved in 200 μL of HFP. A 10 μL aliquot of this solution was placed over a glass substrate along with 10 μL of 10^{-4} g L^{-1} of MPS-PPV potassium salt in water, prepared from the dilution of the commercial solution 0.25/wt % in water (Sigma-Aldrich). The solvent was removed in an oven at 45 °C for 48 h and, then, stored at 6 °C. The system was also prepared in an Eppendorf flask by taking 200 μL of the MPS-PPV solution and adding it to a Phe−Phe solution and left to self-assemble. It was stored at low temperature.

System Sm5—Phe−Phe structures produced in THF with PVK as the additive: (0.53 ± 0.01) mg of Phe−Phe was dissolved in 200 μL of HFP. A 10 μL aliquot of this solution was placed over a glass substrate, and immediately, the same volume of the 10^{-2} g L^{-1} PVK solution was added to it. The solvent was removed in an oven at 45 °C for 30 min and stored at 6 °C. Then, 200 μL of the PVK solution was added to the Eppendorf flask containing the Phe−Phe solution to self-assemble.

Characterization. Scanning electronic micrographs were recorded in a SEM JEOL, JSM-6610 microscope, coupled to energy-dispersion energy Thermo scientific NSS Spectral Imaging. A Denton Vacuum, Desk V was used for gold layer deposition.

Steady-state excitation and fluorescence spectra were recorded in a Fluorolog 3-221 HORIBA Jobin Yvon spectrophotometer, with a 450 W Xe arc-lamp, connected to a double monochromator, with a sample holder adapted for solid samples, in which glass substrates were placed in a 45° right angle with respect to the incident radiation. Emission was detected at 90° by a Hamamatsu photomultiplier, operating at the range of 250−850 nm. Narrow slits were employed to ensure the resolution of 1.0 nm to the measurements. Data from steady-state spectroscopy performed for all samples inform about the energies of excitation and emission of each system, and they are used to determine the emission region in which the fluorescence lifetime should be examined.

TRES was performed under time-correlated single photon counting (TCSPC) measurements and were carried out in a Horiba FluoroMax 4 equipped with a TCSPC hub and NanoLEDs of 345 and 375 nm, with a pulse width of typically 70 ps and with a maximum width of less than 200 ps. Measurements were performed in 4096 channels, which result in time resolutions varying from 3.7 to 4.2 ps for samples presented in this work. They were used to register fluorescence

DOI: 10.1021/acsomega.8b02732
ACS Omega 2019, 4, 606−619

lifetimes in distinct range of wavelengths, determined by the steady-state fluorescence and excitation spectra, but typically at the range of 360−420 nm for the Sm1 sample consisting solely of Phe−Phe self-assembled structures; 360−600 nm for samples containing PPV derivatives as additives (Sm2 and Sm4) and of 360−450 nm for samples containing carbazole derivatives as additives (Sm3 and Sm5). Samples were purged with $N_{2(g)}$ for $O_{2(g)}$ removal and then submitted to dynamic vacuum to be sealed in quartz cuvettes. They were placed in the sample holder to register the fluorescence lifetimes. Data collected for each sample and the instrumental response were deconvoluted and analyzed by the exponential series method. For deconvolution, LUDOX (Sigma-Aldrich) was used as a scatterer. Experimental data correspond to expected theoretical values when the exponential fit adjustment parameter (χ^2) is close to 1.[70]

Computational Simulations. Theoretical calculations were performed using three units of the Phe−Phe monomer. Phe−Phe trimers in neutral and zwitterion forms were optimized at the AM1 semiempirical level of calculation, and the equilibrium geometries were characterized by vibrational frequencies. The calculations were performed in vacuum, THF, and water. Solvent effects were introduced taking into account the polarized continuum model,[71−73] considering water and THF as the environment. All calculations were performed by Gaussian 09 software package.[74]

■ ASSOCIATED CONTENT

Supporting Information

The Supporting Information is available free of charge on the ACS Publications website at DOI: 10.1021/acsomega.8b02732.

Steady-state and time-resolved fluorescence spectroscopy results of the isolated additives MEH-PPV, 9Cz, and PVK (PDF)

■ AUTHOR INFORMATION

Corresponding Author

*E-mail: tatiana@ufg.br. Phone: +55-62-3521-1097 ext. 259. Fax: +55-62-6521-1313 (T.D.M.).

ORCID

Rogério Custódio: 0000-0002-1824-2521

Tatiana D. Martins: 0000-0003-1209-9143

Notes

The authors declare no competing financial interest.

■ ACKNOWLEDGMENTS

The authors thank LABMic/UFG for SEM images, FAPEG for scholarships and financial support to this project, and CNPq (grant 407619/2013-5) for financial support.

■ REFERENCES

(1) Li, D.; Jia, X.; Cao, X.; Xu, T.; Li, H.; Qian, H.; Wu, L. Controllable Nanostructure Formation through Enthalpy-Driven Assembly of Polyoxometalate Clusters and Block Copolymers. *Macromolecules* **2015**, *48*, 4104−4114.

(2) Zhang, J. L.; Zhong, S.; Zhong, J. Q.; Niu, T. C.; Hu, W. P.; Wee, A. T. S.; Chen, W. Rational Design of Two-Dimensional Molecular Donor-Acceptor Nanostructure Arrays. *Nanoscale* **2015**, *7*, 4306−4324.

(3) Kumar-Krishnan, S.; Prokhorov, E.; de Fuentes, O. A.; Ramírez, M.; Bogdanchikova, N.; Sanchez, I. C.; Mota-Morales, J. D.; Luna-Bárcenas, G. Temperature-Induced Au Nanostructure Synthesis in a Nonaqueous Deep-Eutectic Solvent for High Performance Electrocatalysis. *J. Mater. Chem. A* **2015**, *3*, 15869−15875.

(4) He, L.; Yang, X.; Zhao, F.; Wang, K.; Wang, Q.; Liu, J.; Huang, J.; Li, W.; Yang, M. Self-Assembled Supramolecular Nanoprobes for Ratiometric Fluorescence Measurement of Intracellular pH Values. *Anal. Chem.* **2015**, *87*, 2459−2465.

(5) Mushnoori, S.; Schmidt, K.; Nanda, V.; Dutt, M. Designing Phenylalanine-Based Hybrid Biological Materials: Controlling Morphology Via Molecular Composition. *Org. Biomol. Chem.* **2018**, *16*, 2499−2507.

(6) Scanlon, S.; Aggeli, A. Self-Assembling Peptide Nanotubes. *NanoToday* **2008**, *3*, 22−30.

(7) Nasouri, K.; Shoushtari, A. M.; Mojtahedi, M. R. M. Thermodynamic Studies on Polyvinylpyrrolidone Solution Systems Used for Fabrication of Electrospun Nanostructures: Effects of the Solvent. *Adv. Polym. Tech.* **2015**, *34*, 21495.

(8) Liu, F.; Sun, J.; Xiao, S.; Huang, W.; Tao, S.; Zhang, Y.; Gao, Y.; Yang, J. Controllable Fabrication of Copper Phthalocyanine Nanostructure Crystals. *Nanotechnology* **2015**, *26*, 225601.

(9) Zhang, Y.; Li, C.; Li, J.; Wang, T.; Zhang, H.; Yu, X. Ferrocenyl-Functionalized Organic-Inorganic Hybrid Silica: A New Kind of Anion Chemsensor Toward Flouride Anion. *J. Organomet. Chem.* **2015**, *783*, 116−119.

(10) Kondorskiy, A. D.; Kislov, K. S.; Lam, N. T.; Lebedev, V. S. Absorption of Light by Hybrid Metalorganic Nanostructures of Elongated Shape. *J. Russ. Laser Res.* **2015**, *36*, 175−192.

(11) Allafchian, A. R.; Moini, E.; Mirahmadi-Zare, S. Z. Flower-Like Self-Assembly of Diphenylalanine for Electrochemical Human Growth Hormone Biosensor. *IEEE Sens. J.* **2018**, *18*, 8979−8985.

(12) Dayarian, S.; Kopyl, S.; Bystrov, V.; Correia, M. R.; Ivanov, M. S.; Pelegova, E.; Kholkin, A. Effect of the Chloride Anions on the Formation of Self-Assembled Diphenylalanine Peptide Nanotubes. *IEEE Transactions on Ultrasonics Engineering* **2018**, *65*, 1563−1570.

(13) Ishikawa, M. S.; Busch, C.; Motzkus, M.; Martinho, H.; Buckup, T. Two-step kinetic model of the self-assembly mechanism for diphenylalanine micro/nanotube formation. *Phys. Chem. Chem. Phys.* **2017**, *19*, 31647−31654.

(14) Dogariu, A.; Vacar, D.; Heeger, A. J. Picosecond Time-Resolved Spectroscopy of The Excited State in a Soluble Derivative of Poly(Phenylene Vinylene): Origin of The Bimolecular Decay. *Phys. Rev. B: Condens. Matter Mater. Phys.* **1998**, *58*, 10218−10224.

(15) Masheter, A. T.; Abiman, P.; Wildgoose, G. G.; Wong, E.; Xiao, L.; Rees, N. V.; Taylor, R.; Attard, G. A.; Baron, R.; Crossley, A.; Jones, J. H.; Compton, R. G. Investigating the Reactive Sites and the Anomalously Large Changes in Surface pKa Values of Chemically Modified Carbon Nanotubes of Different Morphologies. *J. Mater. Chem.* **2007**, *17*, 2616−2626.

(16) Deepak, F.; Tenne, R. Gas-Phase Synthesis of Inorganic Fullerene-Like Structures Andinorganic Nanotubes. *Open Chem. Chem.* **2008**, *6*, 373−389.

(17) Zarbin, A. J. G. Quimica de (nano)materiais. *Quim. Nova* **2007**, *30*, 1469−1479.

(18) Iijima, S. Helical microtubules of graphitic carbon. *Nature* **1991**, *354*, 56−58.

(19) Kroto, H. W.; Heath, J. R.; O'Brien, S. C. O.; Curl, R. F.; Smalley, R. E. C60: Buckminsterfullerene. *Nature* **1985**, *318*, 162−163.

(20) Novoselov, K. S.; Geim, A. K.; Morozov, S. V.; Jiang, D.; Zhang, Y.; Dubonos, S. V.; Grigorieva, I. V.; Firsov, A. A. Electric Field Effect in Atomically Thin Carbon Films. *Science* **2004**, *306*, 666−669.

(21) Ghadiri, M. R.; Granja, J. R.; Milligan, R. A.; McRee, D. E.; Khazanovich, N. Self-assembling organic nanotubes based on a cyclic peptidearchitecture. *Nature* **1993**, *366*, 324−327.

(22) Lee, D. H.; Granja, J. R.; Martinez, J. A.; Severin, K.; Ghadiri, M. R. A self-replicating peptide. *Nature* **1996**, *382*, 525−528.

(23) Kol, N.; Adler-Abramovich, L.; Barlam, D.; Shneck, R. Z.; Gazit, E.; Rousso, I. Self-Assembled Peptide Nanotubes are Uniquely

DOI: 10.1021/acsomega.8b02732
ACS Omega 2019, 4, 606−619

Rigid Bioinspired Supramolecular Structures. *Nano Lett.* **2005**, *5*, 1343−1346.
(24) Amit, M.; Yuran, S.; Gazit, E.; Reches, M.; Ashkenasy, N. Tailor-Made Functional Peptide Self-Assembling Nanostructures. *Adv. Mater.* **2018**, *30*, 1707083.
(25) Li, J.; Geng, S.; Liu, B.; Wang, H.; Liang, G. Self-assembled mechanism of hydrophobic amino acids and β-cyclodextrin based on experimental and computational methods. *Food Res. Int.* **2018**, *112*, 136−142.
(26) Hauptstein, N.; De Leon-Rodriguez, L. M.; Mitra, A. K.; Hemar, Y.; Kavianinia, I.; Li, N.; Castelletto, V.; Hamley, I. W.; Brimble, M. A. Supramolecular Threading of Peptide Hydrogel Fibrils. *ACS Biomater. Sci. Eng.* **2018**, *4*, 2733−2738.
(27) Forte, G.; Messina, G. M. L.; Zamuner, A.; Dettin, M.; Grassi, A.; Marletta, G. Surface-driven first-step events of nanoscale self-assembly for molecular peptide fibers: An experimental and theoretical study. *Colloids Surf., B* **2018**, *168*, 148−155.
(28) Kim, J.; Han, T. H.; Kim, Y.-I.; Park, J. S.; Choi, J.; Churchill, D. G.; Kim, S. O.; Ihee, H. Role of Water in Directing Diphenylalanine Assembly into Nanotubes and Nanowires. *Adv. Mater.* **2010**, *22*, 583−587.
(29) Reches, M.; Gazit, E. Casting metal nanowires within discrete self-assembled peptide nanotubes. *Science* **2003**, *300*, 625−627.
(30) Krylov, A.; Krylova, S.; Kopyl, S.; Kholkin, A. Non-Hydrostatic Pressure-Induced Phase Transitions in Self-Assembled Diphenylalanine Microtubes. *Tech. Phys.* **2018**, *63*, 1311−1315.
(31) Reches, M.; Gazit, E. Self-Assembly of Peptide Nanotubes and Amyloid-Like Structures by Charged-Termini-Capped Diphenylalanine Peptide Analogues. *Isr. J. Chem.* **2005**, *45*, 363−371.
(32) Makam, P.; Gazit, E. Minimalistic Peptide Supramolecular Co-Assembly: Expanding The Conformational Space For Nanotechnology. *Chem. Soc. Rev.* **2018**, *47*, 3406−3420.
(33) Görbitz, C. H. The structure of nanotubes formed by diphenylalanine, the core recognition motif of Alzheimer's β-amyloid polypeptide. *Chem. Commun.* **2006**, 2332−2334.
(34) Lee, J.-H.; Heo, K.; Schulz-Schönhagen, K.; Lee, J. H.; Desai, M. S.; Jin, H.-E.; Lee, S.-W. Diphenylalanine Peptide Nanotube Energy Harvesters. *ACS Nano* **2018**, *12*, 8138−8144.
(35) Arnon, Z. A.; Pinotsi, D.; Schmidt, M.; Gilead, S.; Guterman, T.; Sadhanala, A.; Ahmad, S.; Levin, A.; Walther, P.; Kaminski, C. F.; et al. Opal-like Multicolor Appearance of Self-Assembled Photonic Array. *ACS Appl. Mater. Interfaces* **2018**, *10*, 20783−20789.
(36) Abbas, M.; Xing, R.; Zhang, N.; Zou, Q.; Yan, X. Antitumor Photodynamic Therapy Based on Dipeptide Fibrous Hydrogels with Incorporation of Photosensitive Drugs. *ACS Biomater. Sci. Eng.* **2017**, *4*, 2046−2052.
(37) Safaryan, S.; Slabov, V.; Kopyl, S.; Romanyuk, K.; Bdikin, I.; Vasilev, S.; Zelenovskiy, P.; Shur, V. Y.; Uslamin, E. A.; Pidko, E. A.; et al. Diphenylalanine-Based Microribbons for Piezoelectric Applications via Inkjet Printing. *ACS Appl. Mater. Interfaces* **2018**, *10*, 10543−10551.
(38) Nolan, M. C.; Caparros, A. M. F.; Dietrich, B.; Barrow, M.; Cross, E. R.; Bleuel, M.; King, S. M.; Adams, D. J. Optimising Low Molecular Weight Hydrogels For Automated 3D Printing. *Soft Matter* **2017**, *13*, 8426−8432.
(39) Tao, K.; Makam, P.; Aizen, R.; Gazit, E. Self-Assembling Peptide Semiconductors. *Science* **2017**, *358*, No. eaam9756.
(40) Sun, H.-L.; Chen, Y.; Han, X.; Liu, Y. Tunable Supramolecular Assembly and Photoswitchable Conversion of Cyclodextrin/Diphenylalanine-Based 1D and 2D Nanostructures. *Angew. Chem. Int. Ed.* **2017**, *56*, 7062−7065.
(41) Aydin, M. E.; Yakuphanoglu, F.; Eom, J.-H.; Hwang, D.-H. Electrical characterization of Al/MEH-PPV/p-Si Schottky diode by current-voltage and capacitance-voltage methods. *Phys. B* **2007**, *387*, 239−244.
(42) Kranzelbinder, G.; Nisoli, M.; Stagira, S.; De Silvestri, S.; Lanzani, G.; Müllen, K.; Scherf, U.; Graupner, W.; Leising, G. Cooperative Effects in Blue Light Emission of Poly-(Para-Phenylene)-Type Ladderpolymer. *Appl. Phys. Lett.* **1997**, *71*, 2725−2727.
(43) Samuel, I. D. W.; Rumbles, G.; Collison, C. J.; Friend, R. H.; Moratti, S. C.; Holmes, A. B. Picosecond Time-Resolved Photoluminescence of PPV Derivatives. *Synth. Met.* **1997**, *84*, 497−500.
(44) Martins, T. D.; de Souza, M. I.; Cunha, B. B.; Takahashi, P. M.; Ferreira, F. F.; Souza, J. A.; Fileti, E. E.; Alves, W. A. Influence of pH and Pyrenyl on the Structural and Morphological Control of Peptide Nanotubes. *J. Phys. Chem. C.* **2011**, *115*, 7906−7913.
(45) Aleshin, A. N. Light-Emitting Transistor Structures Based on Semiconducting Polymers and Inorganic Nanoparticles. *Polym. Sci., Ser. C* **2014**, *56*, 47−58.
(46) Ivanov, M. S.; Khomchenko, V. A.; Salimian, M.; Nikitin, T.; Kopyl, S.; Buryakov, A. M.; Mishina, E. D.; Salehli, F.; Marques, P. A. A. P.; Goncalves, G.; et al. Self-Assembled Diphenylalanine Peptide Microtubes Covered by Reduced Graphene Oxide/Spiky Nickel Nanocomposite: An Integrated Nanobiomaterial for Multifunctional Applications. *Mater. Des.* **2018**, *142*, 149−157.
(47) Eckes, K. M.; Baek, K.; Suggs, L. J. Design and Evaluation of Short Self-Assembling Depsipeptides as Bioactive and Biodegradable Hydrogels. *ACS Omega* **2018**, *3*, 1635−1644.
(48) Min, K.-I.; Lee, S.-W.; Lee, E.-H.; Lee, Y.-S.; Yi, H.; Kim, D.-P. Facile Nondestructive Assembly of Tyrosine-Rich Peptide Nanofibers as a Biological Glue for Multicomponent-Based Nanoelectrode Applications. *Adv. Funct. Mater.* **2018**, *28*, 1705729.
(49) Prachumrak, N.; Potjanasopa, S.; Rattanawan, R.; Namuangruk, S.; Jungsuttiwong, S.; Keawin, T.; Sudyoadsuk, T.; Promarak, V. Coumarin-cored carbazole dendrimers as solution-processed non-doped green emitters for electroluminescent devices. *Tetrahedron* **2014**, *70*, 6249−6257.
(50) Zaleckas, E.; Griniene, R.; Stulpinaite, B.; Grazulevicius, J. V.; Liu, L.; Xie, Z.; Schab-Balcerzak, E.; Kamarauskas, E.; Zhang, B.; Grigalevicius, S. Electroactive Polymers Containing Pendant Harmane, Phenoxazine or Carbazole Rings as Host Materials for OLEDs. *Dyes Pigments* **2014**, *108*, 121−125.
(51) Yuan, X.-D.; Liang, J.; He, Y.-C.; Li, Q.; Zhong, C.; Jiang, Z.-Q.; Liao, L.-S. A Rational Design of Carbazole-Based Host Materials with Suitable Spacer Group Towards Highly-Efficient Blue Phosphorescence. *J. Mater. Chem. C* **2014**, *2*, 6387−6394.
(52) Wang, Y.-W.; Xu, J.-P.; Wang, H.; Li, S.-B.; Shi, Q.-L.; Hong, Y.; Jiang, L.-F.; Yuan, H.-C.; Li, L. White Light Electroluminescence from Poly(9-Vinylcarbazole) (PVK)/Zno Nrs/Poly(2-Methoxy-5-(2-Ethylhexyloxy)-1, 4-Phenylenevinylene) (MEH-PPV) Dual Heterojunctions. *Appl. Phys. A: Mater. Sci. Process.* **2014**, *116*, 1921−1925.
(53) Guo, L.; Yang, B.; Wu, D.; Tao, Y.; Kong, Y. Chiral Sensing Platform Based on the Self-Assemblies of Diphenylalanine and Oxalic Acid. *Anal. Chem.* **2018**, *90*, 5451−5458.
(54) Bolat, G.; Abaci, S.; Vural, T.; Bozdogan, B.; Denkbas, E. B. Sensitive Electrochemical Detection Of Fenitrothion Pesticide Based On Self-Assembled Peptide-Nanotubes Modified Disposable Pencil Graphite Electrode. *J. Electroanal. Chem.* **2018**, *809*, 88−95.
(55) Wu, Y.; Wang, F.; Lu, K.; Lv, M.; Zhao, Y. Self-assembled dipeptide-graphene nanostructures onto an electrode surface for highly sensitive amperometric hydrogen peroxide biosensors. *Sens. Actuators, B* **2017**, *244*, 1022−1030.
(56) Su, Y.; Yan, X.; Wang, A.; Fei, J.; Cui, Y.; He, Q.; Li, J. A peony-flower-like hierarchical mesocrystal formed by diphenylalanine. *J. Mater. Chem.* **2010**, *20*, 6734−6740.
(57) Charalambidis, G.; Kasotakis, E.; Lazarides, T.; Mitraki, A.; Coutsolelos, A. G. Self-Assembly Into Spheres of a Hybrid Diphenylalanine-Porphyrin: Increased Fluorescence Lifetime and Conserved Electronic Properties. *Chem.—Eur. J.* **2011**, *17*, 7213−7219.
(58) Guo, C.; Luo, Y.; Zhou, R.; Wei, G. Probing the Self-Assembly Mechanism of Diphenylalanine-Based Peptide Nanovesicles and Nanotubes. *ACS Nano* **2012**, *6*, 3907−3918.
(59) Huang, R.; Su, R.; Qi, W.; Zhao, J.; He, Z. Hierarchical, Interface-Induced Self-Assembly of Diphenylalanine: Formation of Peptide Nanofibers and Microvesicles. *Nanotechnology* **2011**, *22*, 245609.

DOI: 10.1021/acsomega.8b02732
ACS Omega 2019, 4, 606−619

(60) Chaudhary, N.; Singh, S.; Nagaraj, R. Morphology of Self-Assembled Structures Formed by Short Peptides from the Amyloidogenic Protein Tau Depends on the Solvent in which the Peptides Are Dissolved. *J. Pept. Sci.* **2009**, *15*, 675−684.
(61) Demirel, G.; Malvadkar, N.; Demirel, M. C. Control of Protein Adsorption onto Core−Shell Tubular and Vesicular Structures of Diphenylalanine/Parylene. *Langmuir* **2010**, *26*, 1460−1463.
(62) Yan, X.; Zhu, P.; Li, J. Self-Assembly and Application of Diphenylalanine-Based Nanostructures. *Chem. Soc. Rev.* **2010**, *39*, 1877−1890.
(63) Guo, C.; Luo, Y.; Zhou, R.; Wei, G. Probing the Self-Assembly Mechanism of Diphenylalanine-Based Peptide Nanovesicles and Nanotubes. *ACS Nano* **2012**, *6*, 3907−3918.
(64) Quan, S.; Teng, F.; Xu, Z.; Qian, L.; Hou, Y.; Wang, Y.; Xu, X. Solvent and Concentration Effects on Fluorescence Emission in MEH-PPV Solution. *Eur. Polym. J.* **2006**, *42*, 228−233.
(65) Hsu, J.-H.; Fann, W.; Tsao, P.-H.; Chuang, K.-R.; Chen, S.-A. Fluorescence from Conjugated Polymer Aggregates in Dilute Poor Solution. *J. Phys. Chem. A* **1999**, *103*, 2375−2380.
(66) Sumpter, B. G.; Kumar, P.; Mehta, A.; Barnes, M. D.; Shelton, W. A.; Harrison, R. J. Computational Study of The Structure, Dynamics, and Photophysical Properties of Conjugated Polymers and Oligomers Under Nanoscale Confinement. *J. Phys. Chem. B* **2005**, *109*, 7671−7685.
(67) Martins, T. D.; Weiss, R. G.; Atvars, T. D. Z. Synthesis and Photophysical Properties of a Poly(Methyl Methacrylate) Polymer with Carbazolyl Side Groups. *J. Braz. Chem. Soc.* **2008**, *19*, 1450−1461.
(68) Grazulevicius, J. V.; Soutar, I.; Swanson, L. Photophysics of Carbazole-Containing Systems. 3 Fluorescence of Carbazole-Containing Oligoethers in Dilute Solution. *Macromolecules* **1998**, *31*, 4820−4827.
(69) Takahashi, R.; Wang, H.; Lewis, J. P. Electronic Structures and Conductivity in Peptide Nanotubes. *J. Phys. Chem. B* **2007**, *111*, 9093−9098.
(70) Liu, Y. S.; Ware, W. R. Photophysics of Polycyclic Aromatic Hydrocarbons Adsorbed on Silica Gel Surfaces. 1. Fluorescence Lifetime Distribution Analysis: An Ill-Conditioned Problem. *J. Phys. Chem.* **1993**, *97*, 5980−5986.
(71) Cossi, M.; Barone, V.; Cammi, R.; Tomasi, J. Ab initio study of solvated molecules: A new implementation of the polarizable continuum model. *Chem. Phys. Lett.* **1996**, *255*, 327−335.
(72) Miertuš, S.; Tomasi, J. Approximate Evaluations of the Electrostatic Free Energy and Internal Energy Changes in Solution Processes. *Chem. Phys.* **1982**, *65*, 239−245.
(73) Pascual-ahuir, J. L.; Silla, E.; Tuñon, I. GEPOL: An improved description of molecular surfaces. III. A new algorithm for the computation of a solvent-excluding surface. *J. Comp. Chem.* **2004**, *15*, 1127−1138.
(74) Frisch, M. .; Trucks, G. W.; Schlege, l H. B.; et al. *Gaussian 09*, Revision D.01; Gaussian, Inc.: Wallingford CT, 2009.

DOI: 10.1021/acsomega.8b02732
ACS Omega 2019, 4, 606−619